Energy 241 (2022) 122879

Contents lists available at ScienceDirect

Energy

journal homepage: www.elsevier.com/locate/energy

Lithium-ion battery capacity estimation based on battery surface temperature change under constant-current charge scenario

Jufeng Yang [a], Yingfeng Cai [a, *], Chris Mi [b, **]

[a] Automotive Engineering Research Institute, Jiangsu University, 301 Xuefu Road, Zhenjiang, Jiangsu, 212013, China
[b] Department of Electrical and Computer Engineering, San Diego State University, 5500 Campanile Drive, San Diego, CA, 92182, USA

ARTICLE INFO

Article history:
Received 4 May 2021
Received in revised form
23 October 2021
Accepted 9 December 2021
Available online 11 December 2021

Keywords:
Electric vehicles (EVs)
Lithium-ion batteries
Capacity estimation
Differential thermal voltammetry (DTV)
Battery surface temperature change
Temperature curve transformation

ABSTRACT

Accurate estimation of battery actual capacity in real time is crucial for a reliable battery management system and the safety of electrical vehicles. In this paper, the battery capacity is estimated based on the battery surface temperature change under constant-current charge scenario. Firstly, the evolution of the smoothed differential thermal voltammetry (DTV) curves throughout the aging process is analyzed. Then, the change of the battery surface temperature, which is equivalent to the area under the DTV curve, over a specific voltage range is introduced as a direct feature of interest to reflect the battery actual capacity. In addition, the temperature variation transformation is utilized to reduce the influence of the initial battery inconsistency. Lastly, two battery degradation datasets are utilized to validate the proposed method. The maximum root mean-square errors of the estimation results by the reference correlation are less than 20 mAh and 60 mAh for the two employed batteries (respective nominal capacities are 740 mAh and 4800 mAh). Specifically, the mean estimation errors for the respective two batteries are reduced by approximately 24.74% and 39.60% after the temperature variation transformation. The proposed method is further compared with the existing DTV analysis method and demonstrates the superior performance.

© 2021 The Authors. Published by Elsevier Ltd. This is an open access article under the CC BY-NC-ND license (http://creativecommons.org/licenses/by-nc-nd/4.0/).

1. Introduction

Lithium-ion batteries have been extensively used as the energy storage in electric vehicles (EVs) [1–4]. To maximize the battery service life and alleviate the range anxiety, it is critical to monitor the battery state of health (SoH), especially the capacity degradation state, through the battery management system (BMS) [5–7]. Therefore, the accurate estimation of the battery SoH in real time is one of the most important areas in battery research. Recently, the studies on the battery SoH estimation methods can be roughly categorized into two groups, namely model-based and data-driven-based methods.

For the model-based method, the equivalent circuit model or the electrochemical model is usually adopted to characterize the dynamic behavior of a battery, and the battery capacity is considered as the state variable, then the associated filter or observer algorithm is conducted to identify the battery SoH [8,9]. In addition to identifying the health-related parameters directly, another feasible method is to estimate the battery state of charge (SoC) first using the model-based technique. On this basis, the battery capacity is calculated according to the Coulomb counting equation [10,11]. It is worth noting that the estimation accuracy of this kind of method is heavily dependent on the model accuracy. Although the high-fidelity battery model can effectively improve the estimation accuracy, it complicates the relevant matrix operation and makes the on-board microcontroller suffer from an intensive computational burden [6,12].

For the data-driven-based estimation method, the feature of interest (FoI) that reflects the battery capacity loss is firstly extracted from the battery operating data, and then the empirical fitting method [13–15] or the machine learning method [16–18] is used to establish the correlation between the extracted FoI and the battery SoH. Specifically, selecting and identifying the effective FoI is crucial for the accurate estimation of battery SoH. The commonly used FoIs can be divided into direct and indirect ones, as summarized in Fig. 1.

The direct FoIs are usually extracted directly from the battery

* Corresponding author.
** Corresponding author.
E-mail addresses: yjf@ujs.edu.cn (J. Yang), caicaixiao0304@126.com (Y. Cai), cmi@sdsu.edu (C. Mi).

https://doi.org/10.1016/j.energy.2021.122879
0360-5442/© 2021 The Authors. Published by Elsevier Ltd. This is an open access article under the CC BY-NC-ND license (http://creativecommons.org/licenses/by-nc-nd/4.0/).

Nomenclature

A	Battery surface area [m^2]
Cap_{est}	Estimated battery capacity [Ah]
c_p	Heat capacity [J/°C]
h	Heat convection coefficient [W/(m^2°C)]
h_{valley}	Height of $Valley_2$
k_T	Scaling coefficient
$\widehat{k}_T$	Estimated scaling coefficient
m	Battery mass [kg]
N	Data size
$\dot{Q}$	Heat generation rate [W/m^3]
r	Correlation coefficient
r_k	Search radius
T	Battery surface temperature [°C]
T_{env}	Environment temperature [°C]
t	Time [s]
V	Battery terminal voltage [V]
$V_{lim,i}$	Lower limit value of the voltage range [V]
$V_{lim,i+1}$	Upper limit value of the voltage range [V]
V_{OCV}	Open circuit voltage [V]
V_{start}	Battery terminal voltage at the beginning of the constant-current charge process [V]
V_{end}	Battery terminal voltage at the end of the constant-current charge process [V]
x	Independent variable
$\bar{x}$	Mean value of independent variable
y	Observation variable
$\bar{y}$	Mean value of observation variable

Subscripts

act	actual
env	environment
est	estimated
lim	limit
min	minimum
ref	reference
trans	transformed
vari	variation

Greek symbols

Δ	A change in the value

Acronyms

BMS	Battery management system
CC	Constant-current
CV	Constant-voltage
DTV	Differential thermal voltammetry
DVA	Differential voltage analysis
EV	Electric vehicle
FoI	Feature of interest
GPR	Gaussian process regression
ICA	Incremental capacity analysis
LCO	Lithium cobalt oxide
LFP	Lithium iron phosphate
NCA	Nickel cobalt aluminum oxide
NCO	Lithium nickel cobalt oxide
NMC	Nickel manganese cobalt oxide
RMSE	Root mean-square error
SG	Savitzky-Golay
SoC	State of charge
SoH	State of health

operating data, such as voltage, current, temperature, capacity and time. For example, Ref. [16] adopted four features, i.e., the constant-current (CC) charge time, the constant-voltage (CV) charge time, and two slopes of the charge voltage curve at different regions, to comprehensively reflect the battery aging phenomenon, and proposed an improved Gaussian process regression (GPR) model for the SoH estimation. In order to estimate the battery SoH from the partial charging data, Refs. [13,17] selected the charged capacity recorded in a specific voltage region as the FoI, and used the linear regression and the random forest regression to characterize the correlation between the FoI and the battery capacity fade, respectively. In Ref. [18], the duration of the certain voltage interval was

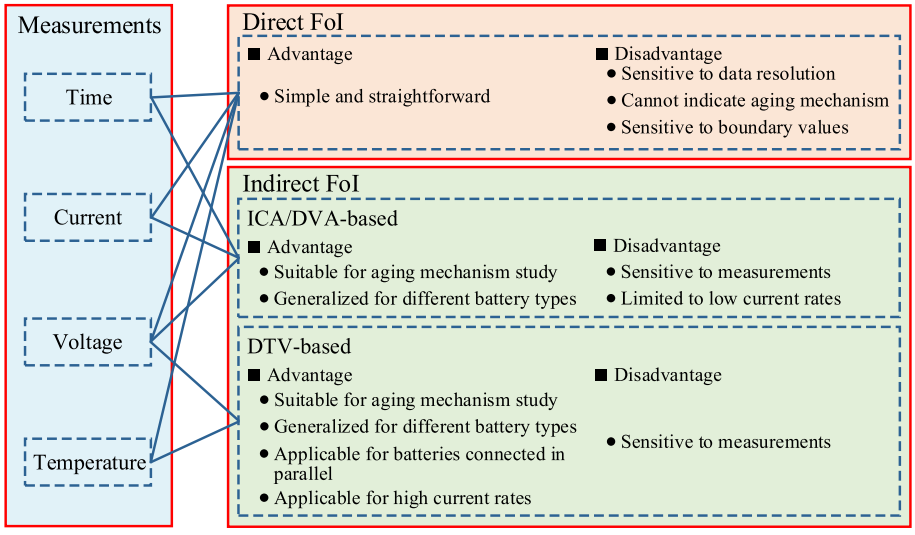

Fig. 1. Summary of commonly used FoIs.

chosen to quantify the battery SoH variation, and a fixed size least squares-based support vector machine with a mixed kernel function was adopted to map the relationship between the extracted FoI and the SoH. As can be seen, it is generally easy and straightforward to extract the direct FoIs. However, the extracted direct FoIs are closely associated with the resolution of the measured data. For example, the number of the recorded features decreases with the increasing measured data interval within a certain range, which may in turn deteriorate the capacity estimation performance [17]. In addition, this kind of FoIs cannot intuitively characterize the battery aging mechanism, and thus trial and error are required to determine the suitable region of the measured data which is strongly correlated with the battery capacity loss. This indicates that the estimation performance is also sensitive to the predefined boundary values, such as the measurement duration [19] and the voltage range [13,17,18].

Different from the direct FoIs, the indirect FoIs are generally obtained based on the differential analysis of the battery operating data during the CC charge and discharge. Generally, the curve parameters, such as the peak/valley location, height, area, and so on, are compared in the differential analysis, and the parameter demonstrating the significant correlation with the battery capacity fade is selected as the indirect FoI. The incremental capacity analysis (ICA) and the differential voltage analysis (DVA) are two frequently used differential analysis methods. These two methods transform the plateau regions in the voltage curve into the identifiable peaks in the incremental capacity (IC)/differential voltage (DV) curve by differentiating the capacity/voltage with respect to the voltage/capacity. The peaks in the IC and DV curves represent the phased transitions in the electrodes and the location of a phase equilibrium, respectively [20,21], and the evolution of the corresponding peak information indicates the degradation mechanism during the battery aging. Hence, ICA/DVA is often used to assist the direct FoI selection [17]. Besides the current and voltage measurements, the temperature data also contain rich characteristic information [22–24]. Hence, in addition to the ICA/DVA, the temperature differential analysis has recently emerged as another effective method to characterize the aging behavior of lithium-ion batteries. There have been a series of studies concerning this technique. For example, Ref. [20] proposed a differential thermal voltammetry (DTV) technique to track the degradation of the nickel manganese cobalt oxide (NMC) cathode battery under the natural convection environment. In Ref. [25], the battery SoH was estimated through the quantitative analysis of the DTV peak evolution, and the results based on the thermal imaging camera measurement indicated that the DTV diagnosis for the employed battery demonstrated no significant dependent on the position of the thermocouple. Furthermore, Ref. [26] extracted four strong-correlation FoIs on the DTV curve, and fed them into the GPR to track the battery capacity degradation. To verify the feasibility of implementing the DTV technique in the real world BMS, Ref. [27] carried out this technique on the battery pack under galvanostatic (dis)charge with forced air convection, which is a more realistic operating condition for EV applications. In Ref. [28], the application of the DTV was extended to the battery with lithium iron phosphate (LFP) chemistry, and the peak-to-peak capacity was found to be a useful FoI to represent the battery capacity fade under the elevated temperature condition. For lithium sulfur battery, which is one of the promising next generation batteries, Ref. [29] demonstrated the feasibility of using the DTV technique to track shuttle during charging. Similar to the DTV analysis technique, Refs. [30,31] extracted the FoI from the differential temperature (DT) curve to identify the battery capacity fade. Generally, the DTV and the DT analysis methods do not require the current measurement. This means that this technique can be applied on the parallel-connected battery pack without the branch current measurement. Compared with the ICA/DVA technique, the DTV/DT technique prefers a higher current rate and does not require isothermal conditions, to guarantee that the battery heat generation dominates over the heat transfer. These indicate that the DTV/DT is a promising online SoH estimation method for practical use. However, due to the numerical differentiation, the IC, DV, DTV, and DT curves will be distorted if obtained directly from the raw data, which are influenced by the noise disturbance, sampling time interval, battery chemistry, and so on. Hence, a series of data processing methods are required, which increases the computational efforts of the on-board BMS.

Considering the aforementioned difficulties, this paper developed a battery capacity estimation method directly based on the measured battery surface temperature under the CC charge scenario. In the proposed framework, the DTV analysis is used to aid the voltage interval determination, then the reference correlation between the decayed battery capacity and the extracted FoI is established offline. Based on the reference correlation, the battery actual capacity can be estimated online when the battery charge voltage covers the determined voltage interval. Besides, the temperature variation transformation is utilized to reduce the influence of the initial battery consistency. Two different battery degradation datasets based on different electrode materials are adopted, and the validation results show that the correlation extracted based on the reference battery can be used to identify the capacity of other batteries in one dataset with a satisfying accuracy, indicating the feasibility of the proposed method.

2. Experimental data analysis

2.1. Dataset description

The test data are based on two types of batteries: (1) eight 740 mAh pouch batteries (numbered from #1 to #8), which consist of a graphite negative electrode and lithium cobalt oxide and lithium nickel cobalt oxide (LCO/NCO) positive electrode [32,33], (2) six 4800 mAh 21,700 batteries (numbered from #9 to #14) with nickel cobalt aluminum oxide (NCA) cathode material. The detailed technical specifications of the employed batteries are listed in Table 1.

Specifically, the LCO/NCO battery degradation dataset is obtained from University of Oxford. Totally eight batteries were cycled by an 8-channel Biologic MPG 205 battery tester, and the batteries were housed in a Binder MK53 thermal chamber at 40 °C. Six NCA batteries were tested by the 16-channel NBT5V20AC16-T battery cycler in one of the authors' laboratory. During the tests, the NCA batteries were placed in a GD-4015 thermal chamber at a constant environment temperature of 25 °C, and the battery surface temperature was monitored and recorded by the PT100 thermocouple. The detailed test procedures for the two types of batteries are presented in Table 2, where C-rate is the measurement of the charge or discharge current with respect to its nominal capacity.

The evolution of the measured battery parameters throughout aging is plotted in Fig. 2. Specifically, the discharged capacities of

Table 1
Technical specifications of tested batteries.

Cathode material	LCO/NCO	NCA
Anode material	Graphite	Graphite
Nominal capacity [mAh]	740	4800
Nominal voltage [V]	3.7	3.6
Charge cutoff voltage [V]	4.2	4.2
Discharge cutoff voltage [V]	2.7	2.5
Weight [g]	19.5 ± 0.5	Max. 69

Table 2
Battery test procedures.

Procedure	LCO/NCO	NCA
1 Cycling tests		
1.1 Charge test	CC charge at 2 C-rate	CCCV charge at 0.5 C-rate
1.2 Discharge test	Artemis drive cycle discharge	CC discharge at 0.5 C-rate
2 Characterization tests		
2.1 Charge test	CC charge at 1 C-rate	CCCV charge at 1 C-rate
2.2 Discharge test	CC discharge at 1 C-rate	CC discharge at 0.5 C-rate
2.3 Pseudo-OCV test	CC charge/discharge at 0.05 C-rate	CC charge/discharge at 0.05 C-rate

LCO/NCO and NCA batteries recorded in the characterization tests are shown in Fig. 2(a) and (b), respectively, and the measured surface temperatures for battery #1 (LCO/NCO) and battery #9 (NCA) at different aging states are exemplarily shown in Fig. 2(c) and (d), respectively. It can be seen from Fig. 2(a) that the discharged capacities of battery #2 and battery #5 dramatically drop at the end of the cycle test. The corresponding battery surface temperatures also present the distinct variation tendency comparing to those in the former cycles. This kind of phenomenon is not studied in this paper and thus the corresponding data are not considered. Besides, as aging progresses, the battery surface temperature curve generally shifts to the lower time level due to the reduced CC charge time, and the variation rate of the battery surface temperature is changed at different aging states, as shown in Fig. 2(c) and (d), indicating that the battery thermal characteristic is closely related to the battery degradation. In addition, it can be concluded from Fig. 2 that compared with the NCA battery degradation dataset, the LCO/NCO battery degradation dataset contains more data points and covers a wider range of capacity loss. Hence, only the LCO/NCO battery degradation dataset is used for the preliminary analysis and the method development.

2.2. DTV curve acquisition

The DTV technology is used in this work to analyze the evolution of the battery characteristics throughout the aging cycles. The DTV parameters can be calculated by differentiating the battery surface temperature with respect to the terminal voltage during CC charge. Furthermore, it can be decoupled to the ratio of temperature and voltage differentials with respect to time, expressed as [20,25]

$$DTV_k = \frac{dT_k}{dV_k} = \frac{T_k - T_{k-1}}{V_k - V_{k-1}} = \frac{T_k - T_{k-1}}{t_k - t_{k-1}} \Big/ \frac{V_k - V_{k-1}}{t_k - t_{k-1}} \tag{1}$$

where T_k and V_k denote the battery surface temperature and terminal voltage measurements during CC charge and discharge at time t_k, respectively. The time interval t_k - t_{k-1} is closely related to the sampling period of the BMS. In this work, the above data are extracted from the 1 C-rate CC charge cycles in the characterization tests.

Generally, the temperature and/or voltage measurements contain noises in a real application, and these interferences will be further amplified by the differential operation if the adopted voltage interval is too small. On the contrary, some useful information will be lost with a large differentiation interval. Since the voltage interval is proportional to the time interval during the CC charge period, the time interval is set as 20 s in this work. Besides, the Savitzky-Golay (SG) filter is adopted to acquire the clear battery surface temperature and DTV curves. The algorithmic procedure of the SG filter is not detailed here but can be referred to Refs. [34,35]. The measured battery terminal voltage and surface temperature are plotted in Fig. 3(a) and (b), respectively. As can be seen, the measured temperature is much noisier than the voltage measurement. Hence, the measured temperature should be smoothed by the SG filter before the differential operation. The processed battery surface temperature and DTV curves are compared to the original curves obtained based on the raw data, as shown in Fig. 3. Specifically, Curve #1 in Fig. 3(b) represents the DTV curve directly calculated based on the measured data, Curve #2 represents the DTV curve calculated based on the filtered battery surface temperature, and Curve #3 represents the DTV curve obtained by further processing Curve #2 with the SG filter. It can be observed from Fig. 3 that with the adopted SG filter and the selected time interval, the noises on the original temperature and DTV curves can be effectively smoothed, and the features on the curves are well preserved, which is critical for the further analysis in the next section.

3. Capacity estimation method

3.1. FoI selection

Based on the aforementioned data smoothing processes, the evolution of DTV curves throughout the aging process is depicted in Fig. 4(a). It can be clearly seen that two valleys ($Valley_1$ and $Valley_2$) and two peaks ($Peak_1$ and $Peak_2$) exist on the acquired DTV curve. The peak/valley height gradually decreases as the battery ages, and the peak/valley position progressively shifts to a higher ($Valley_1$, $Peak_1$ and $Peak_2$) or lower ($Valley_2$) voltage level with the increasing cycle number. Hence, the position-based and the height-based FoIs are commonly employed in the literature to reflect the battery capacity degradation.

Similar to the ICA based methods, the peak/valley area can also be considered as one useful FoI on the DTV curve, since it can capture the changes in the peak/valley shape, as shown in Fig. 4(a). The area under the relevant DTV peak/valley can be expressed as

$$Area_i = \int_{\tau=V_{\mathrm{lim},i}}^{\tau=V_{\mathrm{lim},i+1}} \frac{dT}{dV} d\tau = T(V_{\mathrm{lim},i+1}) - T(V_{\mathrm{lim},i}) = \Delta T_i \tag{2}$$

where $Area_i$ (i = 1–4 in this work) is the area under peak/valley, $V_{\mathrm{lim},i}$ and $V_{\mathrm{lim},i+1}$ are the lower and upper limit values of the voltage range, respectively, $T(V_{\mathrm{lim},i})$ and $T(V_{\mathrm{lim},i+1})$ are the battery surface temperature when V reaches $V_{\mathrm{lim},i}$ and $V_{\mathrm{lim},i+1}$, respectively, and ΔT_i is the corresponding battery surface temperature change.

It can be seen from (2) that $Area_i$ indicates the change of the battery surface temperature in the voltage range of [$V_{\mathrm{lim},i}$, $V_{\mathrm{lim},i+1}$],

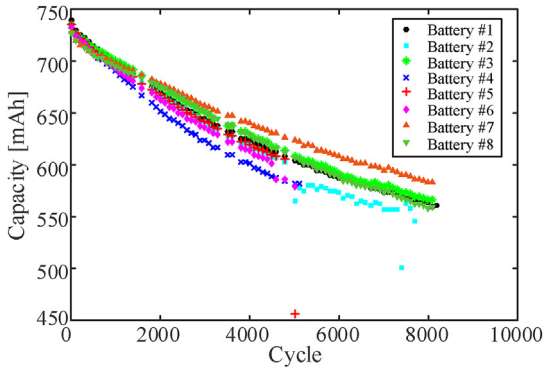

(a)

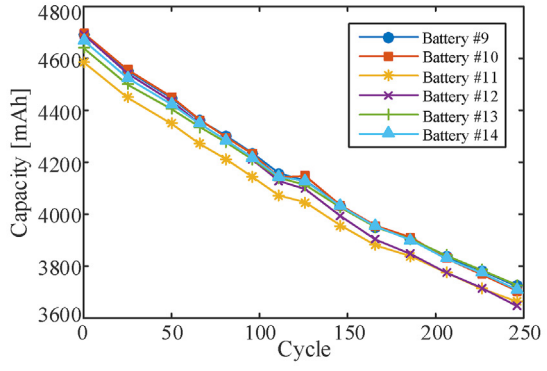

(b)

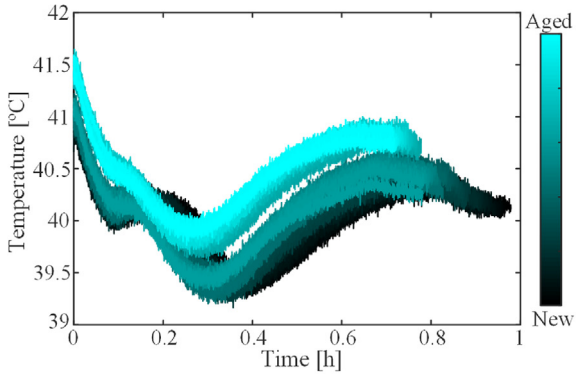

(c)

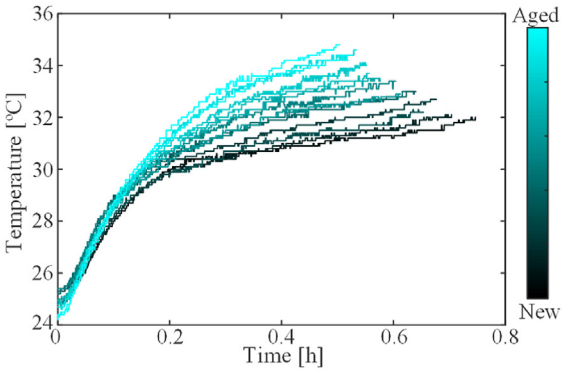

(d)

and the identification of $Area_i$ can be simplified to the calculation of ΔT_i between the battery surface temperatures at $V_{lim,i}$ and $V_{lim,i+1}$. This means that we can directly obtain the FoI from the temperature measurements, instead of extracting the position-based and height-based FoIs from the processed DTV curve. Specifically, the location of $V_{lim,i}$ and the relevant calculation method are schematically demonstrated in Fig. 4(d), where V_{start} and V_{end} represent the battery terminal voltage at the beginning and the end of the CC charge process, respectively, $V_{valleyi}$ and V_{peaki} represent the positions of $Valley_i$ and $Peak_i$, respectively.

The changing trend of the curve area throughout aging varies in different voltage ranges. Take $Peak_1$ as an example, although in a certain aging state, the right part of the peak slightly rises as aging progresses, the left part obviously declines during cycling, resulting in the overall decreasing area, as shown in Fig. 4(b). For $Valley_2$ as shown in Fig. 4(c), the curve variation rates at initial life are generally larger than those at middle and late life, which may cause the different change tendencies of $Area_3$ at different cycling stages, although with the decreasing valley height. This may decrease the monotonicity of the relationship between ΔT_3 and the battery capacity. Hence, it is of great significance to select the appropriate voltage range.

In order to comprehensively and quantitatively investigate the influence of the charge voltage range on the established correlation. The evolutions of capacity for battery #1 with respect to ΔT in the voltage ranges of $[V_{lim,i}, V_{lim,i+1}]$ $(i = 1–4)$ are demonstrated in Fig. 5, and the corresponding correlation coefficients $(r_{x,y})$ are also displayed in the figures. $r_{x,y}$ can be calculated by [36]

$$r_{x,y} = \frac{\sum_{i=1}^{N}(x_i - \overline{x})(y_i - \overline{y})}{\sqrt{\sum_{i=1}^{N}(x_i - \overline{x})^2}\sqrt{\sum_{i=1}^{N}(y_i - \overline{y})^2}}, \overline{x} = \frac{1}{N}\sum_{i=1}^{N}x_i, \overline{y} = \frac{1}{N}\sum_{i=1}^{N}y_i \tag{3}$$

where the independent variable x and the observation y correspond to the selected FoI and the battery capacity, respectively, x and y denote mean values of x and y, respectively, and N represents the data size.

It can be observed from Fig. 5 that the variation of ΔT in the range of $[V_{lim,2}, V_{lim,3}]$ (ΔT_2) is monotonic with respect to the battery capacity, and demonstrates the strongest correlation with the battery capacity, with the highest $|r_{xy}|$ of 0.9729. This is consistent with the aforementioned analysis. Therefore, ΔT_2, which is equivalent to $Area_2$, is selected as the FoI in this work. Besides, the correlation coefficients based on the test data of all eight batteries are listed in Table 3. It can be concluded that ΔT_2 presents the strongest correlation with the battery capacity for all tested batteries (marked with bold characteristic), suggesting the universality of the selected FoI for the batteries in this work.

3.2. Battery surface temperature transformation

Considering the differences among the batteries, the correlation established based on one battery cannot always be applied to other ones. In order to improve the universality of the established

Fig. 2. Evolution of batteries parameters throughout the aging process: capacity fade curves of (a) LCO/NCO batteries at 40 °C and (b) NCA batteries at 25 °C; evolution of battery surface temperature for (c) battery #1 and (d) battery #9 (The line color changes from black to light blue corresponds to the increasing cycle number. For interpretation of the references to color in this figure legend, the reader is referred to the Web version of this article.) (The data of LCO/NCO batteries are obtained from Refs. [32,33].)

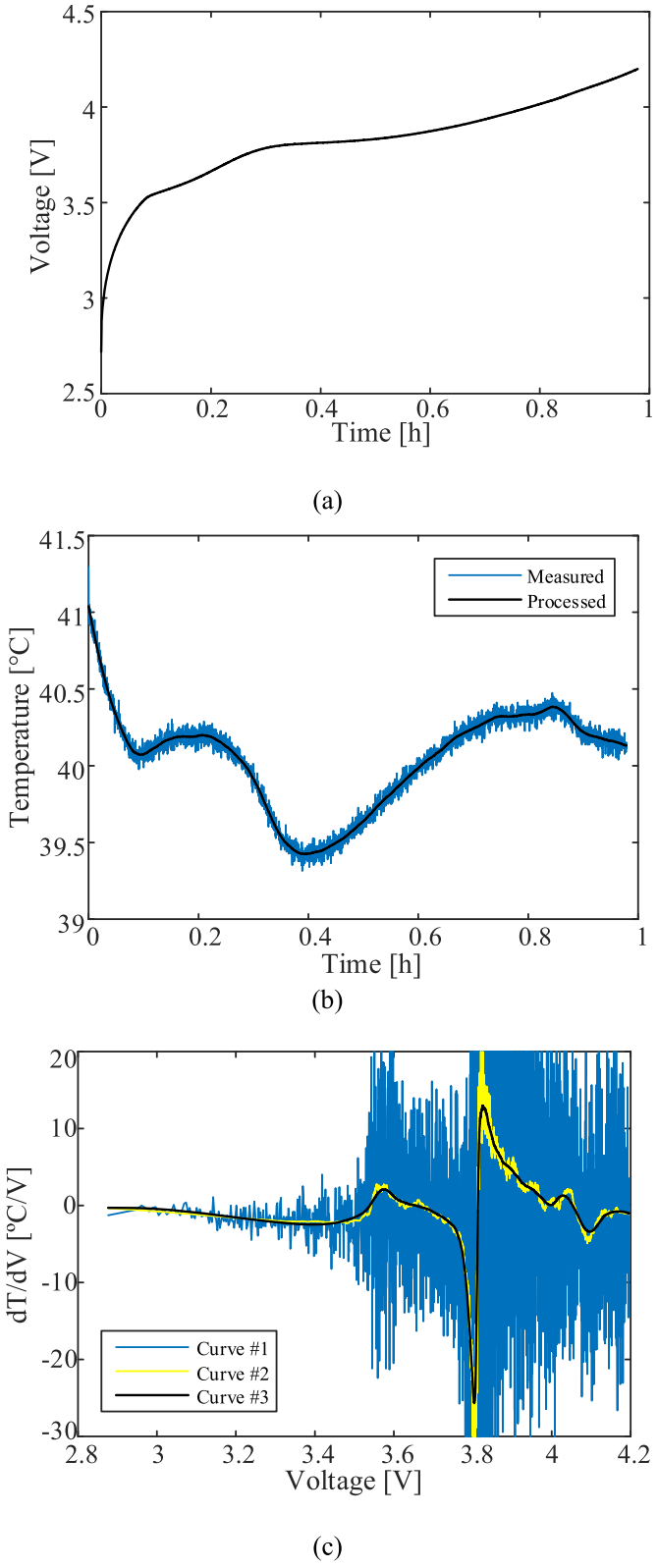

Fig. 3. (a) Measured battery terminal voltage as well as comparison between original and processed curves (b) battery surface temperature; (c) DTV.

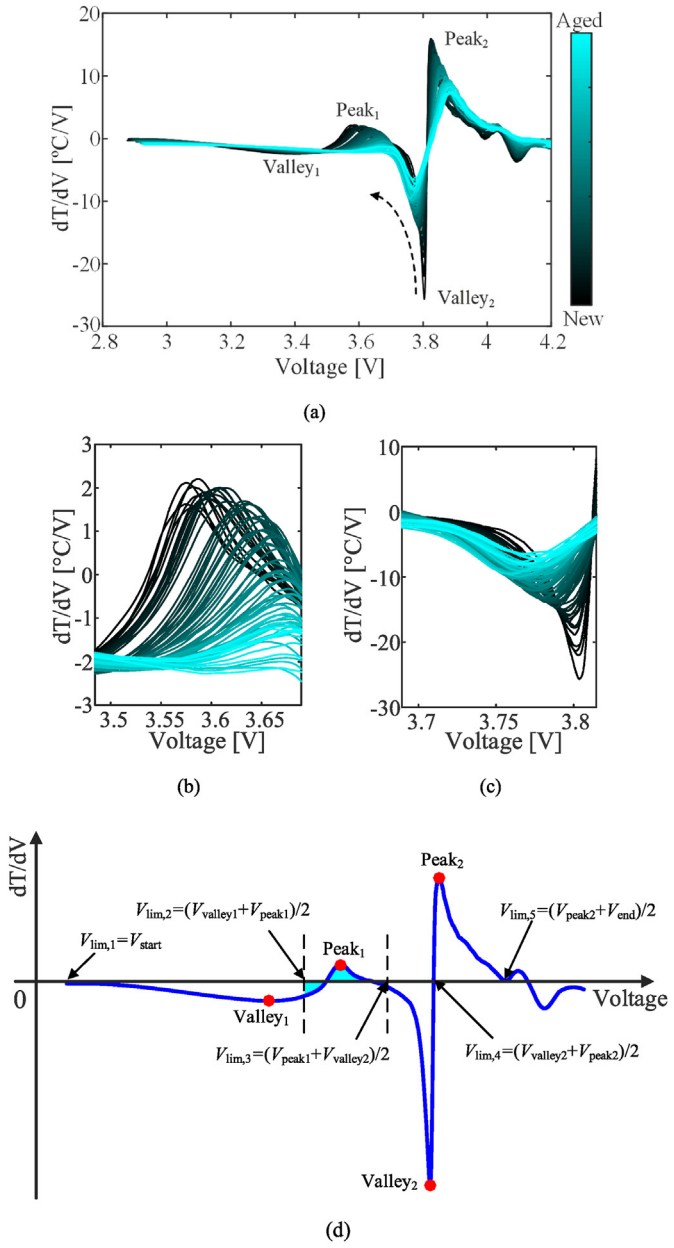

Fig. 4. Evolutions of (a) DTV curves; (b) $Peak_1$ and (c) $Valley_2$ (the line color changes from black to light blue corresponds to the increasing cycle number); (d) schematic representation of different FoIs and voltage ranges (the light blue region corresponds to $Area_2$). (For interpretation of the references to color in this figure legend, the reader is referred to the Web version of this article.)

correlation, a battery surface temperature transformation method is introduced in this section to reduce the influence of battery inconsistency.

The heat generation during the CC charge can be calculated as [37]

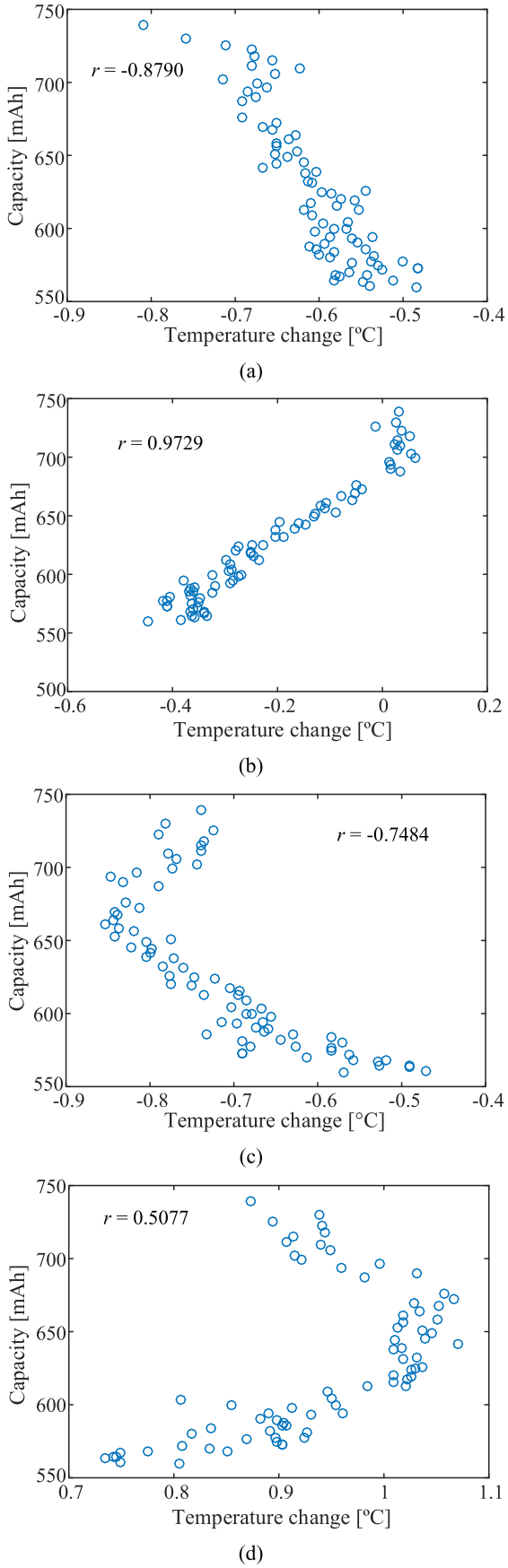

Fig. 5. Evolution of capacity for battery #1with respect to ΔT in the voltage ranges of (a) [$V_{lim,1}$, $V_{lim,2}$]; (b) [$V_{lim,2}$, $V_{lim,3}$]; (c) [$V_{lim,3}$, $V_{lim,4}$]; (d) [$V_{lim,4}$, $V_{lim,5}$].

$$\dot{Q} = I(V - V_{OCV}) + IT\frac{\partial V_{OCV}}{\partial T} \tag{4}$$

where $\dot{Q}$ is the heat generation rate, I is the current, V_{OCV} represents the open circuit voltage.

Assuming the temperature distribution inside the battery is uniform during the charging process, the battery temperature variation rate (dT/dt) can be expressed as (5) based on the lumped thermal model [30,37], where m is the battery mass, c_p is the heat capacity, h is the heat convection coefficient, A is the battery surface area, and T_{env} is the environment temperature.

$$\frac{dT}{dt} = \frac{\dot{Q}}{mc_p} - \frac{hA}{mc_p}(T - T_{env}) \tag{5}$$

Specifically, the second term on the right side of (5) represents the heat loss from the battery surface to the environment. Considering the limited surface temperature change for the new battery in this study, and the generally well-insulated batteries in the vehicle application [38], the influence of heat dissipation on the battery surface temperature variation can be assumed as negligible, and (5) can be rewritten as

$$\frac{dT}{dt} \approx \frac{\dot{Q}}{mc_p} = \frac{I}{mc_p}\left[(V - V_{OCV}) + T\frac{\partial V_{OCV}}{\partial T}\right] \tag{6}$$

where c_p can be considered as a constant due to the limited battery surface temperature change. $(V - V_{OCV}) + T\partial V_{OCV}/\partial T$ in (6) is strongly influenced by the operating temperature, SoC, SoH, battery chemistry, production process, and so on [30,37,39]. It can be concluded that the thermal characteristic of two batteries may be diverse even at the identical aging state, and the dT/dt curves will almost overlap only when the two batteries have similar characteristics. Hence, assuming the batteries at similar SoHs are charged from the same initial SoC, the influence of the battery inconsistency can be reduced by scaling the actual dT/dt curve to the reference curve. As discussed in Section 2, it is difficult to obtain a clear dT/dt curve in the real application due to the measurement disturbance and differential operations. Instead, we can process the temperature variation curve (T-T_{offset}) directly considering $dT/dt = d(T\text{-}T_{offset})/dt$. It should be noted that the battery aging is closely associated with the variation of dT/dt curve, thus only the temperature curves at the beginning of the cycle test, i.e., with similar capacities, are employed to conduct the transformation.

Based on the aforementioned analysis, the battery surface temperature transformation procedure mainly includes two steps. Firstly, the temperature variation values of the reference and actual batteries are obtained by subtracting the offset values from the corresponding measured temperatures, where the offset value is calculated by averaging the battery surface temperature during the CC charge process. Then, the scaling coefficient k_T is determined by minimizing the root mean-square error (RMSE) between the reference temperature variation values ($T_{vari,ref}$) and the actual temperature variation values after transformation ($T_{vari,act,trans}$). The objective function is

$$\widehat{k}_T = \text{argmin}\text{RMSE}(k_T) \tag{7}$$

where $\widehat{k}_T$ is the estimated k_T, and the detailed expression of RMSE (k_T) is

Table 3
Correlation coefficients between capacity and ΔT for eight batteries in different voltage ranges.

Voltage range	Number							
	#1	#2	#3	#4	#5	#6	#7	#8
$[V_{lim,1}, V_{lim,2}]$	−0.8790	−0.4182	−0.8585	−0.9425	−0.4289	−0.9456	−0.6441	−0.9396
$[V_{lim,2}, V_{lim,3}]$	**0.9729**	**0.9700**	**0.9529**	**0.9531**	**0.9094**	**0.9605**	**0.9608**	**0.9773**
$[V_{lim,3}, V_{lim,4}]$	−0.7484	−0.4693	−0.3913	−0.8311	0.4470	−0.3110	0.2757	−0.5332
$[V_{lim,4}, V_{lim,5}]$	0.5077	0.3656	0.1591	0.4308	−0.1535	0.3227	0.4324	0.7830

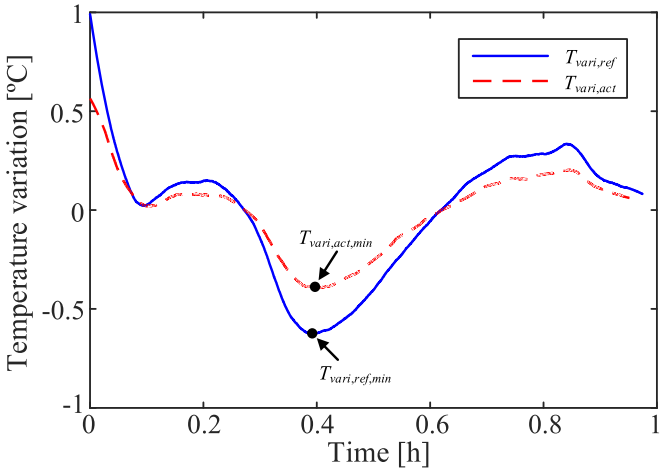

(a)

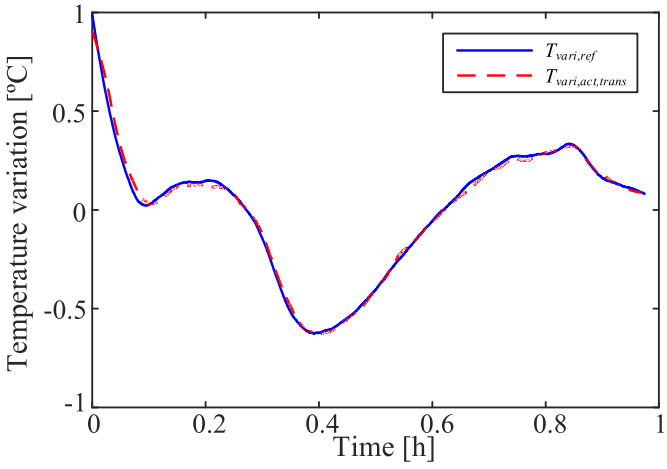

(b)

Fig. 6. Comparison of battery surface temperature variation curves (a) before and (b) after transformation.

$$\begin{cases} \mathrm{RMSE}\left(k_T\right) = \sqrt{\sum_{i=1}^{N}\left[T_{vari,ref,i} - T_{vari,act,trans,i}(k_T)\right]^2 \Big/ N} \\ T_{vari,act,trans,i}(k_T) = k_T T_{vari,act,i} \\ T_{vari,ref,i} = T_{ref,i} - \sum_{i=1}^{N} T_{ref,i} \Big/ N \\ T_{vari,act,i} = T_{act,i} - \sum_{i=1}^{N} T_{act,i} \Big/ N \end{cases} \tag{8}$$

where N is the size of the measured data, and $T_{vari,act,i}$ is the actual temperature value before the transformation, T_{ref} and T_{act} are the reference and actual battery surface temperatures, respectively. Specifically, $T_{vari,act,trans}(k_T)$ is computed based on k_T ranging from $k_{T,0}$-r_k to $k_{T,0}$+r_k, with a certain interval Δk_T, where $k_{T,0}$ and r_k denote the predetermined initial value and search radius, respectively.

The comparisons of battery surface temperature variation curves, as well as the differences between the reference and actual temperature variation curves are exemplarily presented in Fig. 6. In this case, $T_{vari,ref}$ represents temperature variation curves of battery #1, $T_{vari,act}$ and $T_{vari,act,trans}$ represent the temperature variation curves of battery #3 before and after the transformation, respectively. In this study, r_k and Δk_T are set as 0.5 and 0.01, respectively, and $k_{T,0}$ is calculated as

$$k_{T,0} = T_{vari,ref,min} \Big/ T_{vari,act,min} \tag{9}$$

where $T_{vari,ref,min}$ and $T_{vari,act,min}$ are the minimum values of the reference and actual temperature variation, respectively, as illustrated in Fig. 6(a).

The extracted scaling coefficient k_T for battery #3 is 1.5962. It can be seen that the transformed temperature variation curve of battery #3 can well overlap that of the reference battery. In order to quantitatively evaluate the performance of the curve transformation, the obtained k_Ts and the RMSEs for batteries #2 to #8 are presented in Table 4. It can be observed from Table 4 that the discrepancy between the reference and actual temperature variation curves can be effectively reduced after the curve transformation, especially for batteries #3 and #8. Hence, it is feasible to

Table 4
RMSE between reference and actual temperature variation values.

Number		#2	#3	#4	#5	#6	#7	#8
k_T		1.0071	1.5962	1.0352	0.8229	0.7876	0.8587	0.7351
RMSE [°C]	Before	0.0177	0.1206	0.0226	0.0909	0.0916	0.0575	0.1209
	After	0.0175	0.0208	0.0199	0.0613	0.0376	0.0227	0.0332

transform the temperature variation curves by vertical scaling.

3.3. Capacity estimation framework

Based on the aforementioned discussion, the proposed method mainly consists of two parts, i.e., offline extraction and online estimation, as shown in Fig. 7.

The offline extraction part is performed after the test of the selected reference battery. Firstly, the smoothed surface temperatures are obtained based on the test data from the laboratory experiments. Secondly, the complete DTV curves are further acquired through the differential and smoothing operations. Thirdly, the evolution of the DTV curves throughout the aging process is analyzed to determine the area, i.e., the voltage range [$V_{\mathrm{lim},ref,i}$, $V_{\mathrm{lim},ref,i+1}$], demonstrating the strongest correlation with the battery capacity loss. Then, the temperature changes in the selected voltage range (ΔT_{ref}) at different aging states are extracted, and the reference regression function between the battery capacity and ΔT_{ref} is established. When the offline extraction procedure is finished, the battery surface temperatures extracted at the initial characterization test, the voltage range, and the detailed coefficients of the reference regression function are stored in the onboard BMS for the online battery capacity estimation.

The online estimation part is conducted when the battery is operated under the CC charge scenario. In step 1, k_T is identified by comparing the measured temperatures with the stored reference temperatures, as detailed in Section 3.2. Besides, based on the measured data, the actual voltage range [$V_{\mathrm{lim},act,i}$, $V_{\mathrm{lim},act,i+1}$] is determined according to the area selected offline. It should be noted that the temperature transformation and the voltage range determination for each battery are implemented only when the first CC charge process is finished. In step 2, ΔT_{act} is obtained when the battery terminal voltage covers the preset [$V_{\mathrm{lim},act,i}$, $V_{\mathrm{lim},act,i+1}$], and the simple moving average smoothing method can be employed to filter the measurement noises. In step 3, the transformed battery surface temperature change (ΔT_{trans}) is calculated by multiplying the actual one (ΔT_{act}) with the obtained scale factor (k_T), i.e., $\Delta T_{trans} = \Delta T_{act} \times k_T$. In step 4, the battery actual capacity can be obtained by substituting ΔT_{trans} into the established reference regression function.

4. Validation and discussion

4.1. Capacity estimation performance analysis

(1) Influence of temperature transformation: The evolutions of capacity with respect to the temperature change before and after the temperature transformation for eight LCO/NCO batteries are demonstrated in Fig. 8(a) and (b), respectively. In these figures, the solid curves represent the reference correlation extracted based on battery #1, which can be mathematically expressed as

$$Cap_{est} = 112.8\Delta T_{trans}^2 + 362.5\Delta T_{trans} + 696.9 \tag{10}$$

where Cap_{est} represents the estimated battery capacity.

The detailed RMSEs of the battery capacity estimation results are listed in Table 5 for the quantitative evaluation. It can be observed from Fig. 8(a) that for some batteries, the estimated capacities are always higher (such as battery #3) or lower (such as battery #8) than the actual ones, which correspond to relatively large RMSEs (the RMSEs of batteries #3 and #8 can reach as high as

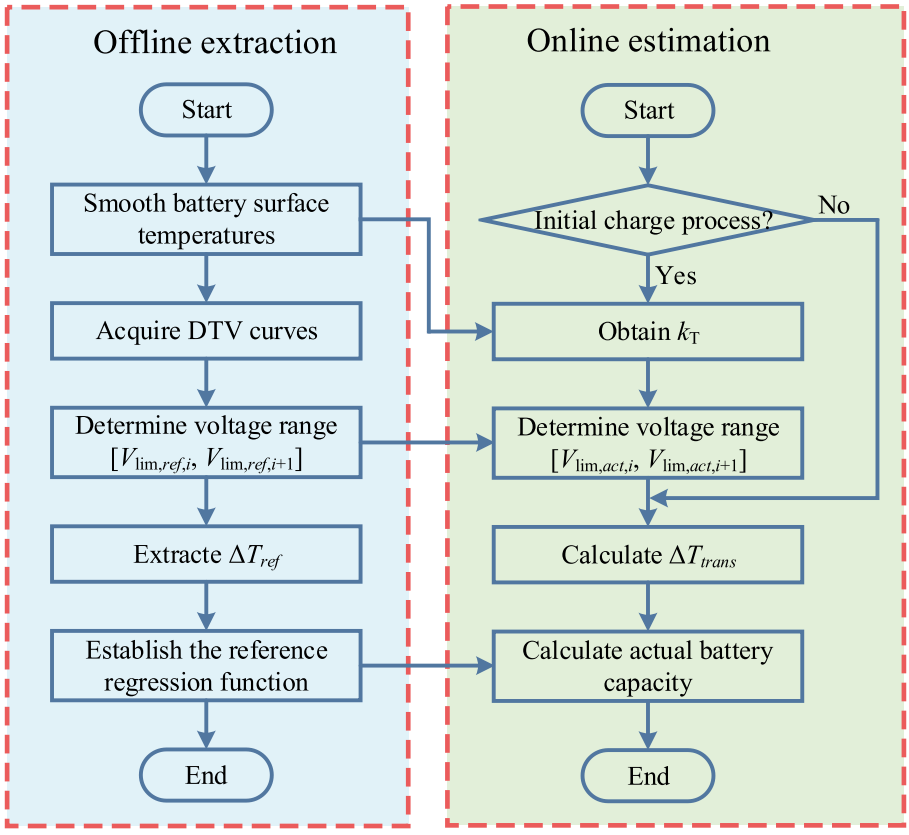

Fig. 7. Proposed ΔT-based capacity estimation framework.

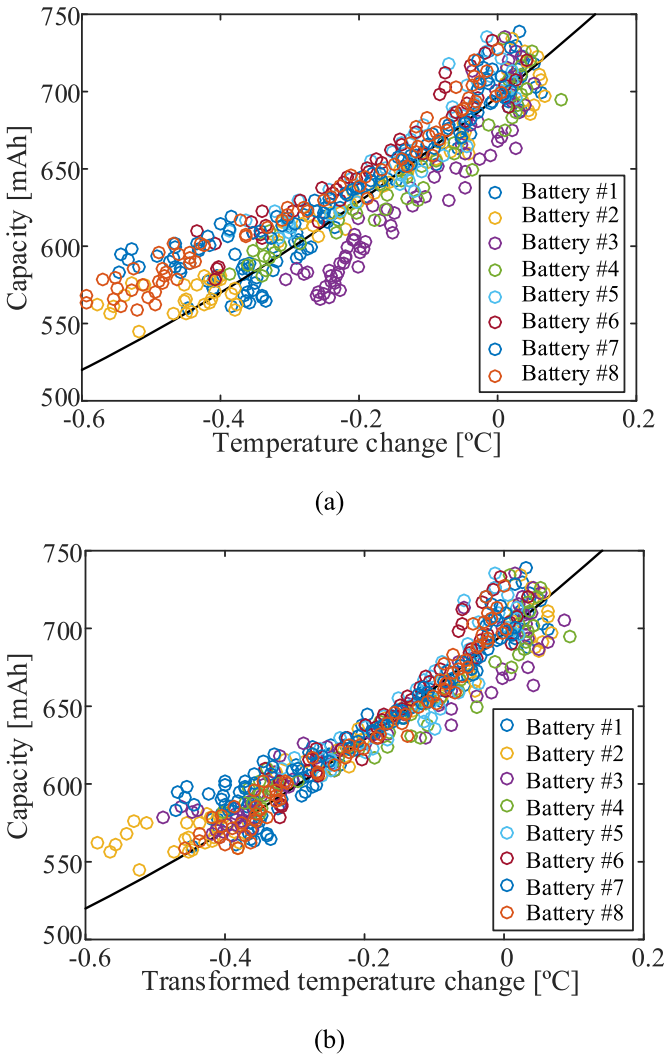

Fig. 8. Evolutions of capacity with respect to the temperature change (a) before and (b) after transformation for eight LCO/NCO batteries (battery #1 as the reference one).

28.49 mAh and 27.19 mAh, respectively). By contrast, the estimated capacities for eight batteries based on the transformed temperature change are closer to the reference correlation curve, and the corresponding RMSEs can be generally reduced within 20 mAh (the battery nominal capacity is 740 mAh), as shown in Table 5. These suggest that the temperature transformation method can effectively reduce the influence of the initial battery inconsistency on the capacity estimation accuracy.

Furthermore, in order to evaluate the overall performance of the proposed method, the mean RMSEs of the capacity estimation results by the reference correlation for eight batteries are summarized in Table 6. The mean RMSE can be calculated as.

Table 6
Mean RMSEs of capacity estimation results by reference correlation based on eight LCO/NCO batteries.

Reference number	Mean RMSE [mAh]		Reference number	Mean RMSE [mAh]	
	Before	After		Before	After
#1	20.75	14.49	#5	21.12	18.94
#2	18.62	14.14	#6	20.84	16.04
#3	34.98	14.84	#7	19.15	16.19
#4	19.35	15.86	#8	19.42	15.68

$$\overline{RMSE} = \sum_{i=1}^{8} RMSE_i / 8 \tag{11}$$

where $\overline{RMSE}$ represents the mean RMSE, $RMSE_i$ represents the RMSE of the capacity estimation results when battery #i is considered as the reference battery. It can be observed that for all eight tested LCO/NCO batteries, the estimation results based on ΔT_{trans} demonstrate a superior accuracy compared to those directly based on ΔT_{act} (the mean estimation error are reduced by approximately 24.74%), validating the universality of the proposed method.

(2) Comparison with the existing DTV analysis method: The DTV analysis method is another efficient temperature-based technique for the battery capacity estimation. Based on the evolution of the smoothed DTV curves as shown in Fig. 4(a), the height of $Valley_2$ is selected as the FoI in this work. The evolutions of the battery capacity with respect to the height of $Valley_2$ before and after the temperature transformation for eight batteries are demonstrated in Fig. 9. Specifically, the valley heights in Fig. 9(b) are extracted from the DTV curves based on the transformed battery surface temperature. Besides, the solid curves in Fig. 9 represent the reference correlation extracted based on battery #1, and are expressed as

$$Cap_{est} = -0.4756h_{valley}^2 - 26.36h_{valley} + 387.6 \tag{12}$$

where h_{valley} represents the height of $Valley_2$.

The RMSEs of the capacity estimation results by (12) are listed in Table 7. It can be observed from Fig. 9 and Table 7 that the estimation error can be effectively reduced after the temperature transformation. Especially for batteries #3 and #8, the corresponding RMSEs decrease from 65.79 mAh and 58.17 mAh to 16.37 mAh and 11.47 mAh, respectively. The results indicate that the proposed temperature transformation method can also be applied on the DTV analysis technique with a satisfying estimation accuracy.

In addition, the performances of the existing DTV analysis method and the proposed ΔT-based method are compared in Fig. 10, where the mean RMSEs of the estimation results by the reference correlations based on all the tested LCO/NCO batteries are

Table 5
RMSEs of capacity estimation results by reference correlation based on battery #1.

Number	RMSE [mAh]		Number	RMSE [mAh]	
	Before	After		Before	After
#1	11.65	11.65	#5	19.47	15.67
#2	15.09	15.38	#6	22.84	14.02
#3	28.49	17.32	#7	26.34	16.63
#4	14.91	15.10	#8	27.19	10.13

Table 7
RMSEs of capacity estimation results by reference correlation based on battery #1.

Number	RMSE [mAh]		Number	RMSE [mAh]	
	Before	After		Before	After
#1	10.57	10.57	#5	39.00	14.98
#2	24.56	25.42	#6	28.45	17.00
#3	65.79	16.37	#7	41.17	20.34
#4	12.59	8.65	#8	58.17	11.47

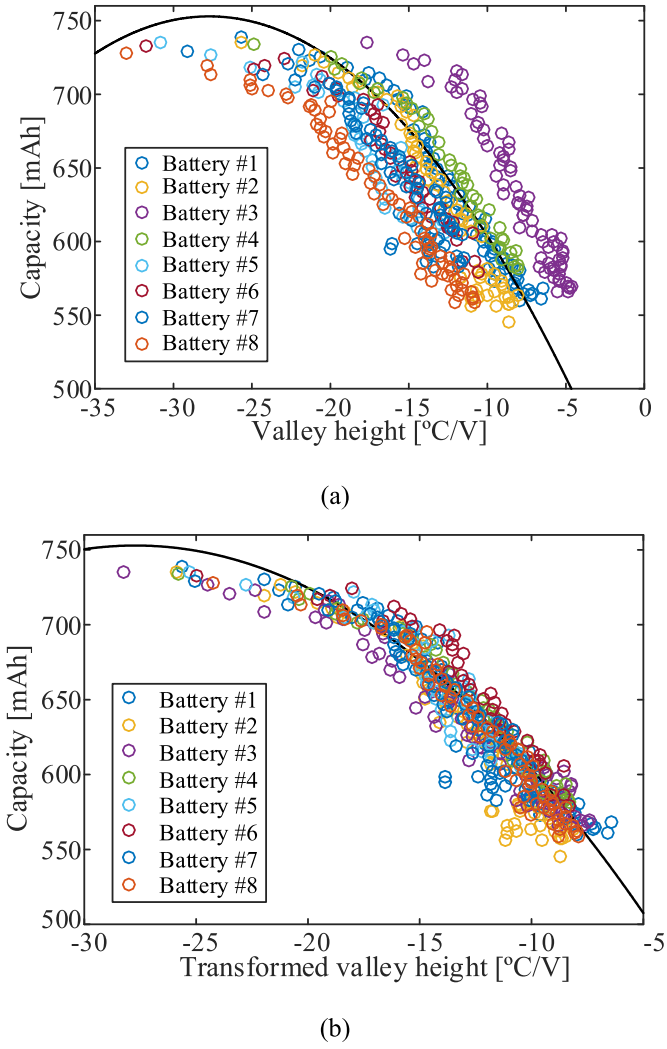

Fig. 9. Evolutions of capacity with respect to the valley height (a) before and (b) after transformation for eight LCO/NCO batteries (battery #1 as the reference one).

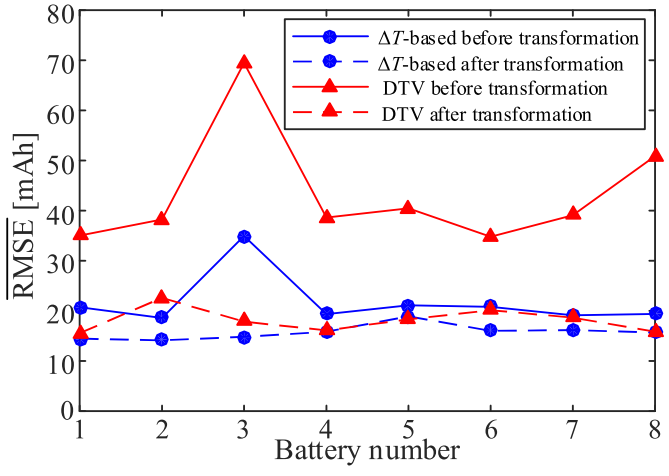

Fig. 10. Comparison of capacity estimation results between DTV and Δ*T*–based methods.

displayed to make a straightforward comparison. It can be seen that: (1) the Δ*T*-based method generally outperforms the DTV analysis method, even in the condition that the temperature transformation is not conducted; (2) the temperature transformation method is useful to reduce the influence of the initial battery inconsistency on the estimation accuracy for both methods; (3) the proposed method demonstrates the superior accuracy, i.e., the lowest $\overline{RMSE}$, in most cases.

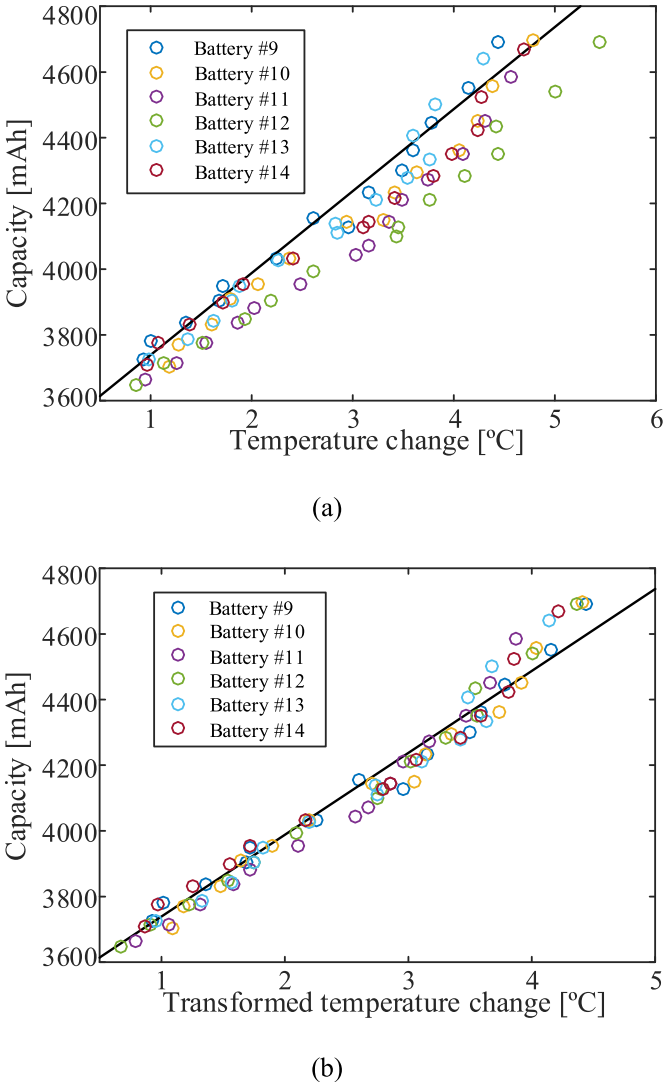

Fig. 11. Evolutions of capacity with respect to the temperature change (a) before and (b) after transformation for six NCA batteries (battery #9 as the reference one).

4.2. Validation on NCA battery degradation dataset

Six groups of battery aging data from the NCA battery degradation dataset are employed in this section to further validate the universality of the proposed method.

Firstly, the appropriate voltage ranges are determined based on the correlation analysis. Then, the battery capacity estimation results are obtained and compared in Fig. 11(a) and (b). In these figures, battery #9 is considered as the reference battery, and the linear regression function, expressed as (13), is employed for the capacity estimation.

$$Cap_{est} = 249.51\Delta T_{trans} + 3489 \tag{13}$$

It can be observed from Fig. 11 that compared with the estimated capacities without the temperature transformation, the

Table 8
Mean RMSEs of capacity estimation results by reference correlation based on six NCA batteries.

Reference number	Mean RMSE [mAh]		Reference number	Mean RMSE [mAh]	
	Before	After		Before	After
#9	99.54	52.36	#12	99.27	49.87
#10	73.44	50.12	#13	87.52	49.98
#11	86.86	53.42	#14	73.12	53.16

estimation results after the transformation are closer to the reference correlation curve, which is similar to the results obtained based on the LCO/NCO battery test data. Besides, in the case of constructing the reference regression functions based on the test data of different batteries, the corresponding mean RMSEs of the estimated capacities are listed in Table 8. It can be concluded that the overall mean RMSEs are reduced approximately 39.60% for the employed NCA batteries after the temperature transformation.

5. Conclusion

A battery capacity estimation method is developed in this paper, which is based on the change of the battery surface temperature during the specific charge voltage interval. Besides, the temperature variation curve transformation is proposed to reduce the initial battery thermal inconsistency. Compared with the existing DTV analysis method, the proposed ΔT-based method presents the following advantages.

(1) More easily obtained FoI. Due to the measurement noise, the pre-smoothing step is necessary to extract the useful information in the DTV curve. For the proposed method, the DTV analysis is only required to determine the appropriate voltage range offline. While in the online estimation procedure, only the battery surface temperatures corresponding to $V_{\mathrm{lim},act,i}$ and $V_{\mathrm{lim},act,i+1}$ are required to calculate ΔT directly, which effectively reduces the computational burden and enables a fast SoH estimation.
(2) Improved universality. With the temperature transformation, the established reference correlation based on one battery can be applied to other batteries with an enhanced accuracy. Specifically, the mean RMSEs are reduced by approximately 24.74% and 39.60% for the tested LCO/NCO and NCA batteries, respectively.

It should be noted that besides the battery inconsistency, the noise interference and the measurement resolution of the thermocouple also have a significant impact on the estimation accuracy of the battery actual capacity. In addition, the feasibility of the proposed method in the low ambient temperature has not been verified in this paper. Therefore, the aforementioned influences will be considered in the future work to improve the adaptivity of the developed method for real application.

Credit author statement

Jufeng Yang: Conceptualization, Software, Data curation, Validation, Writing – original draft, Writing – review & editing, Funding acquisition. **Yingfeng Cai:** Supervision, Project administration. **Chris Mi:** Supervision, Methodology, Writing – review & editing.

Declaration of competing interest

The authors declare that they have no known competing financial interests or personal relationships that could have appeared to influence the work reported in this paper.

Acknowledgments

The authors would like to acknowledge the funding support from the China Postdoctoral Science Foundation (2020M671356), the Natural Science Foundation of Jiangsu Province (BK20210773), and the National Natural Science Foundation of China (U1764257).

References

[1] Mi C, Masrur MA. Hybrid electric vehicles: principles and applications with practical perspectives. John Wiley & Sons; 2017.
[2] Deng Z, Hu X, Lin X, Kim Y, Li J. Sensitivity analysis and joint estimation of parameters and states for all-solid-state batteries. IEEE Trans Transport Electrification 2021;7:1314–23.
[3] Akhoundzadeh MH, Panchal S, Samadani E, Raahemifar K, Fowler M, Fraser R. Investigation and simulation of electric train utilizing hydrogen fuel cell and lithium-ion battery. Sustain Energy Technol Assessment 2021;46:101234.
[4] Tran M-K, Bhatti A, Vrolyk R, Wong D, Panchal S, Fowler M, et al. A review of range extenders in battery electric vehicles: current progress and future perspectives. World Electric Vehicle J 2021;12:54.
[5] Panchal S, Mcgrory J, Kong J, Fraser R, Fowler M, Dincer I, et al. Cycling degradation testing and analysis of a LiFePO4 battery at actual conditions. Int J Energy Res 2017;41:2565–75.
[6] Xiong R, Li L, Tian J. Towards a smarter battery management system: a critical review on battery state of health monitoring methods. J Power Sources 2018;405:18–29.
[7] Deng Z, Hu X, Lin X, Xu L, Che Y, Hu L. General discharge voltage information enabled health evaluation for lithium-ion batteries. IEEE ASME Trans Mechatron 2020;26:1295–306.
[8] Hu X, Yuan H, Zou C, Li Z, Zhang L. Co-estimation of state of charge and state of health for lithium-ion batteries based on fractional-order calculus. IEEE Trans Veh Technol 2018;67:10319–29.
[9] Chen C, Xiong R, Shen W. A lithium-ion battery-in-the-loop approach to test and validate multiscale dual H infinity filters for state-of-charge and capacity estimation. IEEE Trans Power Electron 2018;33:332–42.
[10] Shen P, Ouyang M, Lu L, Li J, Feng X. The Co-estimation of state of charge, state of health, and state of function for lithium-ion batteries in electric vehicles. IEEE Trans Veh Technol 2018;67:92–103.
[11] Hu X, Jiang H, Feng F, Liu B. An enhanced multi-state estimation hierarchy for advanced lithium-ion battery management. Appl Energy 2020;257:114019.
[12] Yang J, Xia B, Shang Y, Huang W, Mi CC. Adaptive state-of-charge estimation based on a split battery model for electric vehicle applications. IEEE Trans Veh Technol 2017;66:10889–98.
[13] Tang X, Zou C, Yao K, Chen G, Liu B, He Z, et al. A fast estimation algorithm for lithium-ion battery state of health. J Power Sources 2018;396:453–8.
[14] Stroe D, Schaltz E. Lithium-ion battery state-of-health estimation using the incremental capacity analysis technique. IEEE Trans Ind Appl 2020;56:678–85.
[15] Jiang B, Dai H, Wei X. Incremental capacity analysis based adaptive capacity estimation for lithium-ion battery considering charging condition. Appl Energy 2020;269:115074.
[16] Yang D, Zhang X, Pan R, Wang Y, Chen Z. A novel Gaussian process regression model for state-of-health estimation of lithium-ion battery using charging curve. J Power Sources 2018;384:387–95.
[17] Li Y, Zou C, Berecibar M, Nanini-Maury E, Chan JCW, van den Bossche P, et al. Random forest regression for online capacity estimation of lithium-ion batteries. Appl Energy 2018;232:197–210.
[18] Shu X, Li G, Zhang Y, Shen J, Chen Z, Liu Y. Online diagnosis of state of health for lithium-ion batteries based on short-term charging profiles. J Power Sources 2020;471:228478.
[19] Richardson RR, Birkl CR, Osborne MA, Howey DA. Gaussian process regression for in situ capacity estimation of lithium-ion batteries. IEEE Trans Industrial Inform 2018;15:127–38.
[20] Wu B, Yufit V, Merla Y, Martinez-Botas RF, Brandon NP, Offer GJ. Differential thermal voltammetry for tracking of degradation in lithium-ion batteries. J Power Sources 2015;273:495–501.
[21] Gong X, Xiong R, Mi CC. A data-driven bias-correction-method-based lithium-ion battery modeling approach for electric vehicle applications. IEEE Trans Ind Appl 2016;52:1759–65.
[22] Tomaszewska A, Chu Z, Feng X, O'Kane S, Liu X, Chen J, et al. Lithium-ion battery fast charging: a review. eTransportation 2019;1:100011.
[23] Mevawalla A, Panchal S, Tran M-K, Fowler M, Fraser R. One dimensional fast computational partial differential model for heat transfer in lithium-ion batteries. J Energy Storage 2021;37:102471.

[24] Zhu W, Weng Z, Li Y, Zhang L, Zhao B, Xie C, et al. Theoretical analysis of shape factor on performance of annular thermoelectric generators under different thermal boundary conditions. Energy 2021;239:122285.
[25] Merla Y, Wu B, Yufit V, Brandon NP, Martinez-Botas RF, Offer GJ. Novel application of differential thermal voltammetry as an in-depth state-of-health diagnosis method for lithium-ion batteries. J Power Sources 2016;307:308–19.
[26] Wang Z, Yuan C, Li X. Lithium battery state of health estimation via differential thermal voltammetry with Gaussian process regression. IEEE Trans Transport Electrification 2020;7:16–25.
[27] Merla Y, Wu B, Yufit V, Brandon NP, Martinez-Botas RF, Offer GJ. Extending battery life: a low-cost practical diagnostic technique for lithium-ion batteries. J Power Sources 2016;331:224–31.
[28] Shibagaki T, Merla Y, Offer GJ. Tracking degradation in lithium iron phosphate batteries using differential thermal voltammetry. J Power Sources 2018;374:188–95.
[29] Hua X, Zhang T, Offer GJ, Marinescu M. Towards online tracking of the shuttle effect in lithium sulfur batteries using differential thermal voltammetry. J Energy Storage 2019;21:765–72.
[30] Wu Y, Jossen A. Entropy-induced temperature variation as a new indicator for state of health estimation of lithium-ion cells. Electrochim Acta 2018;276:370–6.
[31] Tian J, Xiong R, Shen W. State-of-Health estimation based on differential temperature for lithium ion batteries. IEEE Trans Power Electron 2020;35:10363–73.
[32] Birkl C. Oxford Battery Degradation Dataset 1: long term battery ageing tests of 8 Kokam (SLPB533459H4) 740 mAh lithium-ion pouch cells. University of Oxford; 2017.
[33] Birkl C. Diagnosis and prognosis of degradation in lithium-ion batteries. University of Oxford; 2017.
[34] Li X, Yuan C, Wang Z. Multi-time-scale framework for prognostic health condition of lithium battery using modified Gaussian process regression and nonlinear regression. J Power Sources 2020;467:228358.
[35] Gong X. Modeling of lithium-ion battery considering temperature and aging uncertainties. University of Michigan-Dearborn; 2016.
[36] Yang J, Xia B, Huang W, Fu Y, Mi C. Online state-of-health estimation for lithium-ion batteries using constant-voltage charging current analysis. Appl Energy 2018;212:1589–600.
[37] Liu G, Ouyang M, Lu L, Li J, Han X. Analysis of the heat generation of lithium-ion battery during charging and discharging considering different influencing factors. J Therm Anal Calorim 2014;116:1001–10.
[38] Wang C-Y, Zhang G, Ge S, Xu T, Ji Y, Yang X-G, et al. Lithium-ion battery structure that self-heats at low temperatures. Nature 2016;529:515–8.
[39] Han X, Lu L, Zheng Y, Feng X, Li Z, Li J, et al. A review on the key issues of the lithium ion battery degradation among the whole life cycle. eTransportation 2019;1:100005.